



**HAL**  
open science

## Silver containing nanostructures from hydrogen-bonded supramolecular scaffolds

Sachin S Kinge, Mercedes Crego-Calama, Maria Peter, David N Reinhoudt

► **To cite this version:**

Sachin S Kinge, Mercedes Crego-Calama, Maria Peter, David N Reinhoudt. Silver containing nanostructures from hydrogen-bonded supramolecular scaffolds. *Supramolecular Chemistry*, 2008, 20 (06), pp.593-600. 10.1080/10610270701537888 . hal-00513515

**HAL Id: hal-00513515**

**<https://hal.science/hal-00513515>**

Submitted on 1 Sep 2010

**HAL** is a multi-disciplinary open access archive for the deposit and dissemination of scientific research documents, whether they are published or not. The documents may come from teaching and research institutions in France or abroad, or from public or private research centers.

L'archive ouverte pluridisciplinaire **HAL**, est destinée au dépôt et à la diffusion de documents scientifiques de niveau recherche, publiés ou non, émanant des établissements d'enseignement et de recherche français ou étrangers, des laboratoires publics ou privés.



**Silver containing nanostructures from hydrogen-bonded supramolecular scaffolds**

Journal:	<i>Supramolecular Chemistry</i>
Manuscript ID:	GSCH-2007-0083.R1
Manuscript Type:	Full Paper
Date Submitted by the Author:	20-Jun-2007
Complete List of Authors:	Kinge, Sachin; University Twente, SMCT crego-calama, mercedes; University Twente, SMCT Peter, Maria; University Twente, SMCT Reinhoudt, David; University Twente, SMCT
Keywords:	hydrogen bonds, supramolecular chemistry, self-assembly, surface templation, nanorods



# Silver containing nanostructures from hydrogen-bonded supramolecular scaffolds

SACHIN. KINGE, MARIA PÉTER, MERCEDES CREGO-CALAMA, ‡\*

and DAVID. N. REINHOUDT\*

Laboratory of Supramolecular Chemistry and Technology, MESA<sup>+</sup> Institute for Nanotechnology,  
University of Twente, P.O. Box 217, 7500 AE Enschede, The Netherlands.

‡ Present address: Stichting IMEC Nederland, PO Box 8550, 5605 KN, Eindhoven,  
The Netherlands.

\* Correspondence author E-mail: [Mercedes.CregoCalama@imec-nl.nl](mailto:Mercedes.CregoCalama@imec-nl.nl), Phone: +31(0)40 2774119.

Fax: +31(0)40 2746400

**The self-organisation of silver-containing hydrogen-bonded rosette assemblies on highly oriented pyrolytic graphite (HOPG) surfaces is described. The introduction of silver atoms into the double rosette architecture was achieved using the affinity of silver cations for cooperative  $\pi$ -donors or cyano- functionalities on the double rosettes. Highly ordered 2-D nanorod domains with an inter-row spacing of 4-5 nm oriented in different directions were revealed by tapping-mode atomic force microscopy (AFM). This new and simple strategy for the creation of metal-containing supramolecular nanorod arrays that can act as well-defined surface-immobilized self-assembled scaffolds, will contribute to the development of functionalized nanoarchitectures via bottom-up approaches.**

*Keywords:* Hydrogen-bonds; Supramolecular chemistry; Self-assembly; Templatation - silver complexation; Nano-domains.

## INTRODUCTION

Self-assembly and self-organisation of small building blocks is at the heart of bottom-up approaches [1] as an alternative to currently employed costly lithography based top-down methods of micro- nanofabrication [2] for engineering large-scale ensembles of nanoarchitectures [3]. As a natural phenomenon in biological [4] and chemical processes,[5] self-assembly offers attractive possibilities for creating functional molecular structures, for example artificial molecular machines [6]. Recent research interests are focused towards the fabrication, and specially positioning of noncovalent supramolecular aggregates on surfaces in organized networks [7-11]. Though many examples of supramolecular structures formed *in situ* on surfaces are known, only few superstructures formed in solution have been efficiently transferred onto surfaces [7,9, 11e, 12]. In this line our group has reported the synthesis and characterisation of multi-component, hydrogen bonded assemblies (rosette) and their ordered rod-like arrangement on the graphite surfaces [13]. The rosette assemblies are based on the self-assembly of calix[4]arene dimelamines and barbituric acid (or cyanuric acid) derivatives (Figure 1), which are held together by complementary hydrogen-bonding between the donor-acceptor-donor (DAD) array of calix[4]arene dimelamine derivatives and the acceptor-donor-acceptor (ADA) array of the BAR (barbituric acid) or CYA (cyanuric acid) counterparts [13]. These assemblies can be easily functionalised [13d]. Metal-containing self-assembled nanostructures are very interesting for growing metal nanoparticles or creating metallic nanowires from usual biological templates like DNA [16] and peptide nanotubes [17]. Metal atoms bound to the template surface act as nucleating centres for further growth of nanoparticles or can be ‘developed’ by using

1  
2  
3  
4  
5 standard photographic techniques. In this realm, we have previously achieved the  
6 incorporation of gold atoms in the rosette assemblies using coordination to phosphane  
7 groups, which are placed on the melamine part of the rosettes as an alternative non-  
8 biological pathway for creating metallic structures [13c]. However, this pathway includes  
9 the multi-step synthesis of gold substituted calix[4]arene dimelamine derivatives, which  
10 is a costly and a lengthy process. In this article we report an alternative pathway of  
11 organizing metal-containing assemblies on surfaces without need for multi-step synthesis  
12 of metal functionalized precursors. This pathway is based on the use of strong affinity of  
13 certain metal ions for example  $\text{Ag}^+$  ions for cooperative  $\pi$ -donor or cyano- functionalities  
14 easily grafted on the double rosette motifs [18].  
15  
16  
17  
18  
19  
20  
21  
22  
23  
24  
25  
26  
27  
28  
29  
30

31 **[Insert Figure 1 here]**  
32  
33  
34  
35

36 Here we report the 2-D self-assembly of silver functionalized double rosette  
37 assemblies  $\text{Ag}^+ \cdot [\mathbf{1a}_3 \bullet (\text{DEB})_6]$  and  $\text{Ag}^+ \cdot [\mathbf{1b}_3 \bullet (\text{CNPhCYA})_6]$  (Figure 1) on highly oriented  
38 pyrolytic graphite (HOPG) surfaces studied by atomic force microscopy (AFM). AFM is  
39 a very versatile and practical method for studying such self-assembled systems on  
40 surfaces [14]. AFM images show regular 2-D nanorod domains formed from these metal  
41 containing supramolecular nanostructures. Different organisations are observed  
42 depending upon the building blocks DEB (5,5'-diethyl barbiturate) and CNPhCYA (p-  
43 cyano phenyl cyanurate). The silver functionalized double rosette assemblies,  
44  $\text{Ag}^+ \cdot [\mathbf{1a}_3 \bullet (\text{DEB})_6]$  and  $\text{Ag}^+ \cdot [\mathbf{1b}_3 \bullet (\text{CNPhCYA})_6]$  were formed  $[\mathbf{1a}_3 \bullet (\text{DEB})_6]$  and  
45  $[\mathbf{1b}_3 \bullet (\text{CNPhCYA})_6]$  double rosette assemblies with  $\text{Ag}^+ \text{CF}_3 \text{COO}^-$ . These double rosette  
46  
47  
48  
49  
50  
51  
52  
53  
54  
55  
56  
57  
58  
59  
60

1  
2  
3  
4  
5 assemblies are molecular boxes that consist of two flat and circular self-assembled rosette  
6 motifs connected through three calix[4]arene diamelamine moieties via the formation of  
7 36 hydrogen bonds [13] (Figure 1). Employing such templates to direct the formation of  
8 metallic nanostructures may lead in the future to versatile routes to fabricate electrically  
9 conducting nanowires.  
10  
11  
12  
13  
14  
15

## 16 17 18 19 20 21 22 23 24 25 26 27 28 29 30 31 32 33 34 35 36 37 38 39 40 41 42 43 44 45 46 47 48 49 50 51 52 53 54 55 56 57 58 59 60

**EXPERIMENTAL SECTION**

All experiments were performed under argon atmosphere. 5,5'-diethyl barbiturate (DEB) (Aldrich), 2,5-dihydroxybenzoic acid (DHB) (Aldrich) and  $\text{Ag}^+\text{CF}_3\text{COO}$  (ACROS) was purchased and used as received. Calix[4]arene diamelamine derivatives **1a**, **1b** and CNPhCYA were synthesized according to the previous protocol.<sup>1</sup>  $^1\text{H}$  NMR spectra were recorded in  $\text{CDCl}_3$  on a Varian Unity 300. Chemical shifts are given in ppm relative to tetramethylsilane (TMS). Matrix-Assisted Laser Desorption Ionisation (MALDI) Time-of-Flight (TOF) mass spectra were recorded on a Voyager-DE-RP mass spectrometer (Applied Biosystems/PerSeptive Biosystems, Inc., Framingham, MA, USA) equipped with delayed extraction. A 337 nm UV nitrogen laser producing 3-ns pulses was used and the mass spectra were obtained in the linear and reflectron mode. Tapping mode AFM (TM-AFM) thin-film samples were prepared by deposition of one drop of a solution (0.1 mM) of silver complexed assemblies  $\text{Ag}^+\cdot[\mathbf{1a}_3\bullet(\text{DEB})_6]$  and  $\text{Ag}^+\cdot[\mathbf{1b}_3\bullet(\text{CNPhCYA})_6]$  in toluene onto freshly cleaved highly-oriented pyrolytic graphite (HOPG) in a near-saturated atmosphere of toluene. After the solvent was evaporated, the samples were treated for 15 min in oil pump vacuum to remove any traces of residual solvent. The TM-AFM data were acquired with a Nanoscope III multimode AFM (Digital Instruments,

1  
2  
3  
4  
5 Santa Barbara, CA, USA) by using a 10  $\mu\text{m}$  (E) scanner and microfabricated silicon  
6  
7 tips/cantilevers (model TESP, resonance frequency of 300 kHz, Nanosensors, Wetzlar,  
8  
9 Germany). The system was thermally equilibrated over the period of typically 1 to 2 days  
10  
11 by operating the AFM in contact mode with false engagement. The rms amplitude of the  
12  
13 cantilever ( $\approx 0.8$  V) and the amplitude damping ( $\approx 5\%$ ) were minimized to reduce the  
14  
15 peak normal forces. Height, phase, and amplitude images were captured using scan rates  
16  
17 between 0.5 and 3.0 Hz. All data presented here have been subject to a first order plane  
18  
19 fit to compensate for the sample tilt.  
20  
21  
22  
23

#### 24 25 26 **Synthesis of $\text{Ag}^+$ complexes of the hydrogen-bonded assemblies [18]**

27  
28 5-10 mM solutions of the hydrogen-bonded assemblies [ $\mathbf{1a}_3 \bullet (\text{DEB})_6$ ] and  
29  
30 [ $\mathbf{1b}_3 \bullet (\text{CNPhCYA})_6$ ] in  $\text{CHCl}_3$  were stirred for 24 h at room temperature with 1.5  
31  
32 equivalent of  $\text{Ag}^+ \text{CF}_3 \text{COO}^-$ . Further an aliquot of this solution (10 mL) was mixed with  
33  
34 an aliquot (30 mL) of a solution of 2,5-dihydroxybenzoic acid (DHB) ( $3 \text{ mgL}^{-1}$ ) in  
35  
36  $\text{CHCl}_3$ . A portion (1 mL) of the resulting solution was loaded on a gold-sample plate, the  
37  
38 solvent removed in warm air, and the sample transferred to the mass spectrometer for  
39  
40 analysis.  
41  
42  
43  
44  
45  
46  
47  
48  
49  
50  
51  
52  
53  
54  
55  
56  
57  
58  
59  
60

## RESULTS AND DISCUSSION

### Synthesis and characterisation of silver-functionalized double rosettes

Two different silver functionalized double rosette assemblies (Figure 1) were synthesized. The synthesis of double rosette assemblies was performed according to the previous protocol by easily mixing calix[4]arene dimelamine derivatives **1a** (or **1b**) with DEB (5,5-diethyl barbituric acid) or CNPhCYA (*p*-cyano-phenyl cyanuric acid) in 1:2 ratio in apolar solvents chloroform or toluene [19]. The formation of the assemblies is characterized by  $^1\text{H}$  NMR. The characteristic signals around 13-15 ppm of hydrogen-bonded imide protons (-NH) on barbituric acid or cyanuric acid derivatives confirm the formation of the double rosette assemblies (Figure 2b,c). Silver atoms can be easily incorporated in the double rosette assemblies **1a<sub>3</sub>•(DEB)<sub>6</sub>** and **1b<sub>3</sub>•(CNPhCYA)<sub>6</sub>** by reacting 5-10 mM solution of double rosette assemblies ( $\text{CHCl}_3$ ) with 1.5 equivalents of  $\text{Ag}^+\text{CF}_3\text{COO}^-$  for 24 h at room temperature. MALDI-TOF analysis of silver functionalized assemblies show intense signals in the spectra at  $m/z = 4278.3$  (calcd. 4276.1 for  $\text{C}_{228}\text{H}_{276}\text{N}_{48}\text{O}_{30} \cdot ^{107}\text{Ag}^+$ ) for assembly  $\text{Ag}^+ \cdot [\mathbf{1a}_3 \bullet (\text{DEB})_6]$  (Figure 2a) and 4347.9 (calcd. 4348.1 for  $\text{C}_{222}\text{H}_{246}\text{N}_{66}\text{O}_{42} \cdot ^{107}\text{Ag}^+$ ) for assembly  $\text{Ag}^+ \cdot [\mathbf{1b}_3 \bullet \text{CNPhCYA}]_6$  indicating the incorporation of silver atoms in the rosette architecture [18].

[Insert Figure 2 here]

Based on literature results, in the assembly  $\text{Ag}^+ \cdot [\mathbf{1a}_3 \bullet (\text{DEB})_6]$ , the silver ions coordinate to benzyl aromatic ring on calix[4]arene dimelamine presumably forming a



sandwich-type complex with the benzyl substituent on the melamine; while in assembly  $\text{Ag}^+ \cdot [\mathbf{1b}_3 \bullet (\text{CNPhCYA})_6]$  the silver ion coordinates to the cyano functionalities on the cyanurate derivative [8,20]. The introduction of the functional groups in the calix[4]arene dimelamine framework and barbituric/cyanuric acid derivatives can be conveniently performed without interfering with the network of hydrogen bonds that holds the double rosette together.

### Atomic Force Microscopy (AFM)

Highly-ordered and regular 2-D arrays of rosette nanostructures were observed after deposition of the rosettes from toluene onto freshly cleaved HOPG surfaces, as unveiled by contact (or tapping) mode AFM (Figure 3). To suppress the 3-D (bulk) crystallisation of the rosettes, slow evaporation of the solvent in a nearly saturated atmosphere of the solvent was ensured. The AFM data was acquired, as described in detail in experimental section, on a thermally fully equilibrated commercial AFM setup using silicon tips. To prevent sample damage, the rms amplitude of the cantilever and the amplitude damping (5%) were minimized. The observed structure is characterized by an inter-row spacing of  $5.1 \pm 0.1$  nm for assembly  $\text{Ag}^+ \cdot [\mathbf{1a}_3 \bullet (\text{DEB})_6]$  (with  $1.0 \pm 0.2$  nm spacing between the neighboring rosettes) and  $4.8 \pm 0.1$  nm for  $\text{Ag}^+ \cdot [\mathbf{1b}_3 \bullet (\text{CNPhCYA})_6]$  (with  $1.0 \pm 0.1$  nm spacing between the neighboring rosettes). The inter-row spacing or heart-to-heart distance [13c] is the separation between two adjacent nanorod structures measured normal to the row direction from centre of one nanorod to another nanorod centre. The observed inter-row distances are function of the substituents as well as the rosette size and suggests that the rosettes are stacked approximately face-to-face in these rows

1  
2  
3  
4  
5 (Figure. 4) [21]. The silver functionalized rosettes also show a characteristic roughness of  
6  
7 the domain edges. This was prominently observed in case of nanorod domains of  
8  
9 assembly  $\text{Ag}^+ \cdot [\mathbf{1b}_3 \bullet (\text{CNPhCYA})_6]$ . This is shown in higher-magnification AFM images  
10  
11 in Figure 3. In addition to the edge roughness, defects such as vacancies were not  
12  
13 observed. Further, the substrate determines the alignment of the nanorod domains on  
14  
15 surface ( $0^\circ$ ,  $60^\circ$ ,  $120^\circ$ ), which is related to the underlying three-fold symmetry of the  
16  
17 HOPG lattice [22]. There are significant differences in the distribution of the nano-rod  
18  
19 domains on the HOPG surfaces. In case of the assembly  $\text{Ag}^+ \cdot [\mathbf{1a}_3 \bullet (\text{DEB})_6]$  the domains  
20  
21 are distinctly separated; while in case of the complex  $\text{Ag}^+ \cdot [\mathbf{1b}_3 \bullet (\text{CNPhCYA})_6]$  crossing  
22  
23 of nanorod domains with different orientations creates extended and evenly distributed  
24  
25 domain patterns. In both the cases the assemblies were oriented in the edge-on manner  
26  
27 (Figure 4). In edge-on fashion inter rosette spacings correspond to the width of double  
28  
29 rosette molecular box; while height measurements correspond to the dimensions of the  
30  
31 box face.  
32  
33  
34  
35  
36  
37  
38  
39  
40  
41  
42  
43  
44  
45  
46  
47  
48  
49  
50  
51  
52  
53  
54  
55  
56  
57  
58  
59  
60

[Insert Figure 3 here]

[Insert Figure 4 here]

1  
2  
3  
4  
5 The roughness characterization [13c] of the observed jagged domain edges along  
6  
7 the rows are of 1.3 (0.1) nm for assembly  $\text{Ag}^+ \cdot [\mathbf{1b}_3 \bullet (\text{DEB})_6]$  and 1.4 (0.1) nm for  
8  
9 assembly  $\text{Ag}^+ \cdot [\mathbf{1b}_3 \bullet (\text{CNPhCYA})_6]$  (Figure 5, 6), indicating the face to face stacking of  
10  
11 double rosettes. In Figure 5 a,b the observed step lengths at the domain edges are plotted  
12  
13 in the histograms for  $\text{Ag}^+ \cdot [\mathbf{1b}_3 \bullet (\text{DEB})_6]$  and  $\text{Ag}^+ \cdot [\mathbf{1b}_3 \bullet (\text{CNPhCYA})_6]$ , respectively. In  
14  
15 Figure 6, the graphs of the peak positions observed in the histograms for different bin  
16  
17 sizes are plotted versus the peak numbers respectively. The linear regressions shows bin  
18  
19 size-independent slopes. From the slopes integer spacings of differences along the rows  
20  
21 of  $1.3 \pm 0.1$  nm and  $1.4 \pm 0.1$  nm were observed for assemblies  $\text{Ag}^+ \cdot [\mathbf{1a}_3 \bullet (\text{DEB})_6]$  and  
22  
23  $\text{Ag}^+ \cdot [\mathbf{1b}_3 \bullet (\text{CNPhCYA})_6]$ , respectively. The spacings are comparable with the dimensions  
24  
25 of individual rosette nanostructures [13c] and suggest that the rosettes stack in the row  
26  
27 direction.  
28  
29  
30  
31  
32  
33  
34  
35  
36  
37  
38

39 [Insert Figure 5 here]  
40  
41  
42  
43  
44  
45

46 [Insert Figure 6 here]  
47  
48  
49  
50  
51  
52  
53  
54  
55  
56  
57  
58  
59  
60

1  
2  
3  
4  
5 The direct real-space observation of the individual rosettes comprising the  
6 nanorod domains was carried out in high-resolution AFM measurements. As shown in  
7 Figure 3, the two-dimensional fast Fourier transform (2-D FFT, inset in Figure 3) shows  
8 reflections that correspond to the inter-row spacing. From an analysis of the 2-D FFTs,  
9 we obtained an oblique lattice structure, which is characterized by  $a = 4.2 \text{ nm} (\pm 0.1 \text{ nm})$ ,  
10  $b = 3.1 (\pm 0.1 \text{ nm})$  and  $\theta = 122 (3^\circ)$  for assembly  $\text{Ag}^+ \cdot [\mathbf{1b}_3 \bullet (\text{DEB})_6]$  and  $a = 4.3 \text{ nm} (\pm 0.1$   
11  $\text{nm})$ ,  $b = 5.1 (\pm 0.1 \text{ nm})$  and  $\theta = 108 (3^\circ)$  for assembly  $\text{Ag}^+ \cdot [\mathbf{1b}_3 \bullet (\text{CNPhCYA})_6]$ . Their unit  
12 cell probably contains three and four double rosette nanostructures respectively, which  
13 corresponds to a formal area requirement of  $5.0 \text{ nm}^2/\text{rosette}$  and the gas-phase minimized  
14 structure possesses an area requirement of  $3.64 \text{ nm}^2/\text{rosette}$  [13c]. These values are in  
15 good agreement with each other considering earlier reports of related double rosettes.  
16  
17  
18  
19  
20  
21  
22  
23  
24  
25  
26  
27  
28  
29  
30  
31  
32  
33  
34  
35  
36

## 37 CONCLUSIONS

38  
39 We have shown that silver atoms can be successfully incorporated into self-assembled,  
40 hydrogen-bonded rosette assemblies based on substituted calix[4]arene dimelamine and  
41 barbiturate (cyanuric) acid moieties. The rosettes formed in solution are very stable and  
42 can be deposited onto solid surfaces to create metal-containing supramolecular  
43 aggregates with nano-sized dimensions ranging from 0-D (individual rosettes) to 2-D  
44 (rosette layers). In these highly ordered nanorod domains, face-to-face stacked rosettes  
45 form parallel rows lying in edge-on fashion on HOPG surface. Our results show the  
46 feasibility of self-assembled hydrogen-bonded assemblies to serve as a scaffold for the  
47  
48  
49  
50  
51  
52  
53  
54  
55  
56  
57  
58  
59  
60

1  
2  
3  
4  
5 formation of metal containing nanorod arrays. Further, platinated and copper  
6  
7 functionalized double rosette assemblies can be similarly obtained as these cations also  
8  
9 show complexation with rosette structures [18b]. Thus, the strategy reported here may  
10  
11 constitute a viable route for the bottom-up fabrication of, for example, conducting  
12  
13 nanowires templated by hydrogen-bonded assemblies.  
14  
15  
16  
17  
18  
19  
20

### 21 *Acknowledgements*

22  
23 This work has been financially supported by ESF-SONS-FunSMARTs project.  
24  
25  
26  
27  
28  
29

### 30 *References*

- 31  
32  
33 [1] (a) Balzani, V.; Credi, A.; Venturi, M. *Chem. Eur. J.* **2002**, *8*, 5524-5532. (b) Service,  
34  
35 R. F. *Science* **2001**, *293*, 782-785. (c) Whitesides, G. M.; Love, J. C. *Sci. Am.* **2001**, 285,  
36  
37 32-41.  
38  
39  
40 [2] (a) Peercy, P. S. *Nature* **2000**, *406*, 1023-1026. (b) Ito, T.; Okazaki, S. *Nature* **2000**,  
41  
42 *406*, 1027- 1031. (c) Walraff, G. M.; Hinsberg, W. D. *Chem. Rev.* **1999**, *99*, 1801-1821.  
43  
44  
45 [3] (a) Supramolecular Chemistry and Self-Assembly, *Science* **2002**, *295*, 2400-2421.  
46  
47 (b) Huang, Y.; Duan, X. F.; Cui, Y.; Lauhon, L. J.; Kim, K. H.; Lieber, C. M. *Science*  
48  
49 **2001**, *294*, 1313-1317. (c) Postma, H. W. C.; Teepen, T.; Yao, Z.; Grifoni, M.; Dekker,  
50  
51 C. *Science* **2001**, *293*, 76-79. (d) Sone, E. D.; Zubarev, E. R.; Stupp, S. I. *Angew. Chem.*  
52  
53 *Int. Ed.* **2002**, *41*, 1705-1709. (f) Feldheim, d. L.; Keating, C. D. *Chem. Soc. Rev.* **1998**,  
54  
55 *27*, 1-12.  
56  
57  
58  
59  
60

- 1  
2  
3  
4  
5 [4] Tsai, C. J.; Ma, B. Y.; Kumar, S.; Wolfson, H.; Nussinov, R. *Crit. Rev. Biochem.*  
6  
7 *Mol. Biol.* **2001**, *36*, 399-433.  
8  
9  
10 [5] (a) Vilar, R. In *Supramolecular Assembly Via Hydrogen Bonds II* **2004**; Vol. *111*, p  
11 85-137. (b) Elemans, J.; Rowan, A. E.; Nolte, R. J. M. *J. Mater. Chem.* **2003**, *13*, 2661-  
12 2670. (c) Keizer, H. M.; Sijbesma, R. P. *Chem. Soc. Rev.* **2005**, *34*, 226-234.  
13  
14  
15 [6] (a) Balzani, V.; Credi, A.; Raymo, F. M.; Stoddart, J. F. *Angew. Chem., Int. Ed.*  
16 **2000**, *39*, 3348-3391. (b) *Molecular Electronics: Science and Technology*; Aviram, A.;  
17 Ratner, M., Eds.; New York Academy of Sciences: New York, 1998 (c) Ball, P. *Nature*  
18 **2000**, *406*, 118-120. (d) Reed, M. A.; Tour, J. M. *Sci. Am.* **2000**, June issue, 68-75.  
19  
20  
21 [7] (a) Yokoyama, T.; Yokoyama, S.; Kamikado, T.; Okuno, Y.; Mashiko, S. *Nature*  
22 **2001**, *413*, 619-621. (b) De Feyter, S.; De Schryver, F. C. *Chem. Soc. Rev.* **2003**, *32*, 139-  
23 150.  
24  
25  
26 [8] Gimzewski, J. K.; Joachim, C. *Science* **1999**, *283*, 1683-1688.  
27  
28  
29 [9] (a) Barth, J. V.; Costantini, G.; Kern, K. *Nature* **2005**, *437*, 671-679. (b) Barth, J. V.;  
30 Weckesser, J.; Cai, C.; Günter, P.; Bürgi, L.; Jeandupeux, O.; Kern, K. *Angew. Chem.,*  
31 *Int. Ed.* **2000**, *39*, 1230-1234.  
32  
33  
34 [10] Auletta, T.; Dordi, B.; Mulder, A.; Sartori, A.; Onclin, S.; Bruinink, C. M.; Nijhuis,  
35 C. A.; Beijleveld, H.; Péter, M.; Schönherr, H.; Vancso, G. J.; Casnati, A.; Ungaro, R.;  
36 Ravoo, B. J.; Huskens, J.; Reinhoudt, D. N. *Angew. Chem., Int. Ed.* **2004**, *43*, 369-373.  
37  
38  
39 [11] (a) Joachim, C.; Gimzewski, J. K.; Aviram, A. *Nature* **2000**, *408*, 541-548. (b)  
40 Jackel, F.; Watson, M. D.; Mullen, K.; Rabe, J. P. *Phys. Rev. Lett.* **2004**, *92*, 188303. (c)  
41 Maoz, R.; Frydman, E.; Cohen, S. R.; Sagiv, J. *Adv. Mater.* **2000**, *12*, 725-731. (d)  
42 Samori, P. *Chem. Soc. Rev.* **2005**, *34*, 551-561.  
43  
44  
45  
46  
47  
48  
49  
50  
51  
52  
53  
54  
55  
56  
57  
58  
59  
60

- 1  
2  
3  
4  
5 [12] (a) Böhringer, M.; Morgenstern, K.; Schneider, W. D.; Berndt, R.; Mauri, F.; De  
6 Vita, A.; Car, R. *Phys. Rev. Lett.* **1999**, *83*, 324-327. (b) Dmitriev, A.; Lin, N.;  
7 Weckesser, J.; Barth, J. V.; Kern, K. *J. Phys. Chem. B* **2002**, *106*, 6907-6912.  
8  
9  
10  
11 [13] (a) Klok, H. A.; Jolliffe, K. A.; Schauer, C. L.; Prins, L. J.; Spatz, J. P.; Moller, M.;  
12 Timmerman, P.; Reinhoudt, D. N. *J. Am. Chem. Soc.* **1999**, *121*, 7154-7155. (b)  
13 Schönherr, H.; Paraschiv, V.; Zapotoczny, S.; Crego-Calama, M.; Timmerman, P.; Frank,  
14 C. W.; Vancso, G. J.; Reinhoudt, D. N. *Proc. Natl. Acad. Sci. U. S. A.* **2002**, *99*, 5024-  
15 5027. (c) van Manen, H. J.; Paraschiv, V.; Garcia-Lopez, J. J.; Schönherr, H.;  
16 Zapotoczny, S.; Vancso, G. J.; Crego-Calama, M.; Reinhoudt, D. N. *Nano Lett.* **2004**, *4*,  
17 441-446. (d) Friggeri, A.; Van Manen, H.-J.; Auletta, T.; Li, X.-M.; Zapotoczny, S.;  
18 Schönherr, H.; Vancso, G. J.; Huskens, J.; Van Veggel, F. C. J. M.; Reinhoudt, D. N. *J.*  
19 *Am. Chem. Soc.* **2001**, *123*, 6388-6395.  
20  
21  
22 [14] (a) *Single Molecule Detection in Solution*; Zander, C., Enderlein, J., Keller, R. A.,  
23 Eds.; Wiley-VCH: Berlin, **2002**. (b) Ambrose, W. P.; Goodwin, P. M.; Jett, J. H.; Van  
24 Orden, A.; Werner, J. H.; Keller, R. A. *Chem. Rev.* **1999**, *99*, 2929-2956. (c) Fotiadis, D.;  
25 Scheuring, S.; Müller, S. A.; Engel, A.; Müller, D. J. *Micron* **2002**, *33*, 385-397. (d)  
26 Mörner, W. E.; Orrit, M. *Science* **1999**, *283*, 1670-1676.  
27  
28  
29 [15] Prins, L. J.; Reinhoudt, D. N.; Timmerman, P. *Angew. Chem., Int. Ed.* **2001**, *40*,  
30 2382-2426.  
31  
32  
33 [16] Braun, E.; Eichen, Y.; Sivan, U.; Ben-Yoseph, G. *Nature* **1998**, *391*, 775-778.  
34  
35  
36 [17] Reches, M.; Gazit, E. *Science* **2003**, *300*, 625-627.  
37  
38  
39 [18] (a) Jolliffe, K. A.; Crego-Calama, M.; Fokkens, R.; Nibbering, N. M. M.;  
40 Timmerman, P.; Reinhoudt, D. N. *Angew. Chem., Int. Ed.* **1998**, *37*, 1247-1251. (b)  
41  
42  
43  
44  
45  
46  
47  
48  
49  
50  
51  
52  
53  
54  
55  
56  
57  
58  
59  
60

1  
2  
3  
4  
5 Timmerman, P.; Jolliffe, K. A.; Crego-Calama, M.; Weidmann, J.-L.; Prins, L. J.;  
6  
7 Cardullo, F.; Snellink-Rueel, B. H. M.; Fokkens, R. H.; Nibbering, N. M. M.; Shinkai, S.;  
8  
9 Reinhoudt, D. N. *Chem. Eur. J.* **2000**, *6*, 4104-4115.

10  
11 [19] Timmerman, P.; Vreekamp, R. H.; Hulst, R.; Verboom, W.; Reinhoudt, D. N.;  
12  
13 Rissanen, K.; Udachin K. A.; Ripmeester, J. *Chem. Eur. J.* **1997**, *3*, 1823-1832.

14  
15 [20] (a) Karas, M.; Bachmann, D.; Bahr, U.; Hillenkamp, F. *Int. J. Mass Spectrom. Ion*  
16  
17 *Processes* **1987**, *78*, 53-68. (d) Hillenkamp, F.; Karas, M. *Anal. Chem.* **1991**, *63*, 1193A-  
18  
19 1203A.

20  
21 [21] Schönherr, H.; Crego-Calama, M.; Vancso, G. J.; Reinhoudt, D. N. In *Encyclopedia*  
22  
23 *of Nanoscience and Nanotechnology*; Schwarz, J. A., Contescu, C., Putyera, K., Eds.;  
24  
25 Marcel Dekker: New York **2004**.

26  
27 [22] <sup>#</sup> There is also 6° deviation between two neighboring nanorod domains. This is  
28  
29 because these assemblies show supramolecular chirality (*D*<sub>3</sub> symmetry). Due to the lack  
30  
31 of any chiral centre in the assemblies these assemblies are present in the form of two  
32  
33 enantiopure domains, which show spontaneous resolution of racemic mixture of *P* and *M*  
34  
35 rosettes.

36  
37 Prins, L. J. *PhD Thesis*, **2001**, University of Twente.  
38  
39  
40  
41  
42  
43  
44  
45  
46  
47  
48  
49  
50  
51  
52  
53  
54  
55  
56  
57  
58  
59  
60



## FIGURE CAPTIONS

**Figure 1.** Synthesis of silver-functionalized double rosette assemblies  $\text{Ag}^+ \cdot [\mathbf{1a}_3 \bullet (\text{DEB})_6]$  and  $\text{Ag}^+ \cdot [\mathbf{1b}_3 \bullet (\text{CNPhCYA})_6]$ .

**Figure 2.** (a) MALDI-TOF MS spectrum of assembly  $\text{Ag}^+ \cdot [\mathbf{1a}_3 \bullet (\text{DEB})_6]$ <sup>18</sup> and (b) <sup>1</sup>H NMR spectra of double rosette assemblies  $[\mathbf{1a}_3 \bullet (\text{DEB})_6]$  and (c)  $[\mathbf{1b}_3 \bullet (\text{CNPhCYA})_6]$  recorded at 300 K in [D]<sup>8</sup>-toluene at 300 MHz.

**Figure 3.** TM-AFM phase images of double rosette-silver complexes  $\text{Ag}^+ \cdot [\mathbf{1b}_3 \bullet (\text{DEB})_6]$  and  $\text{Ag}^+ \cdot [\mathbf{1b}_3 \bullet (\text{CNPhCYA})_6]$  on HOPG deposited in air. Inset shows 2-D FFT. Unit cell obtained from 2-D FFT's of high-resolution AFM images of the nanorod domains of rosettes are also shown. Arrows indicate the alignment of the nanorod domains according to the three-fold symmetry of the underlying graphite.

**Figure 4.** Double rosette assemblies  $\text{Ag}^+ \cdot [\mathbf{1b}_3 \bullet (\text{DEB})_6]$  and  $\text{Ag}^+ \cdot [\mathbf{1b}_3 \bullet (\text{CNPhCYA})_6]$ , lie in edge-on fashion (left) rather than in face-on fashion (right). The double rosette is a *box-like* structure; edge-on orientation denotes lying of the boxes with edges anchored and flat-surfaces vertically positioned; while face-on indicates anchoring of the flat-surfaces. This is well indicated by the height values:  $4.6 \pm 0.1$  nm for  $\text{Ag}^+ \cdot [\mathbf{1a}_3 \bullet (\text{DEB})_6]$  and  $4.3 \pm 0.1$  nm for  $\text{Ag}^+ \cdot [\mathbf{1b}_3 \bullet (\text{CNPhCYA})_6]$ , which correspond to the lateral

1  
2  
3  
4  
5 dimensions of the *box*-face. (Substituents on the assemblies and metal atoms are not  
6  
7 shown for clarity.)  
8  
9

10  
11  
12 **Figure 5.** Histograms of the observed distance-differences at the edge of nanorod  
13 domains obtained by AFM analysis for (a)  $\text{Ag}^+ \cdot [\mathbf{1a}_3 \bullet (\text{DEB})_6]$  (0.25 nm bin size) and (b)  
14  
15  $\text{Ag}^+ \cdot [\mathbf{1b}_3 \bullet (\text{CNPhCYA})_6]$  with Fourier smoothed data (solid lines).  
16  
17  
18

19  
20  
21 **Figure 6.** Plots of observed distance-differences at the edge of nanorod domains for  
22 different bin sizes versus peak number in the histograms analyzed. From the slopes, the  
23  
24 integer spacings of the distance differences are determined for (a)  $\text{Ag}^+ \cdot [\mathbf{1a}_3 \bullet (\text{DEB})_6]$  and  
25  
26  
27 (b)  $\text{Ag}^+ \cdot [\mathbf{1b}_3 \bullet (\text{CNPhCYA})_6]$ .  
28  
29  
30  
31  
32  
33  
34  
35  
36  
37  
38  
39  
40  
41  
42  
43  
44  
45  
46  
47  
48  
49  
50  
51  
52  
53  
54  
55  
56  
57  
58  
59  
60

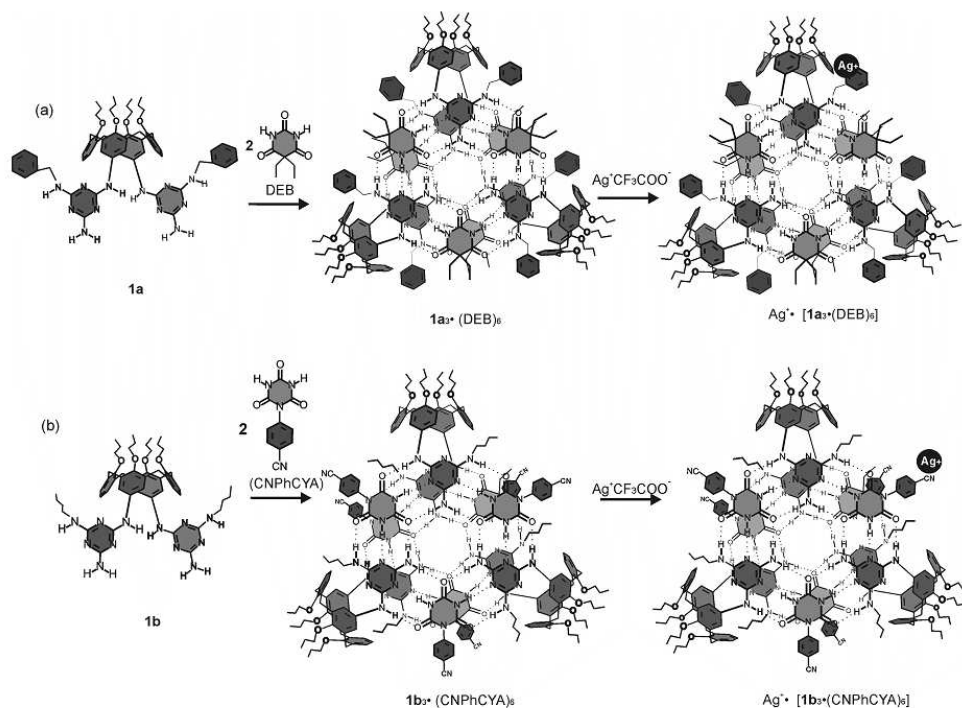


figure1  
254x190mm (96 x 96 DPI)

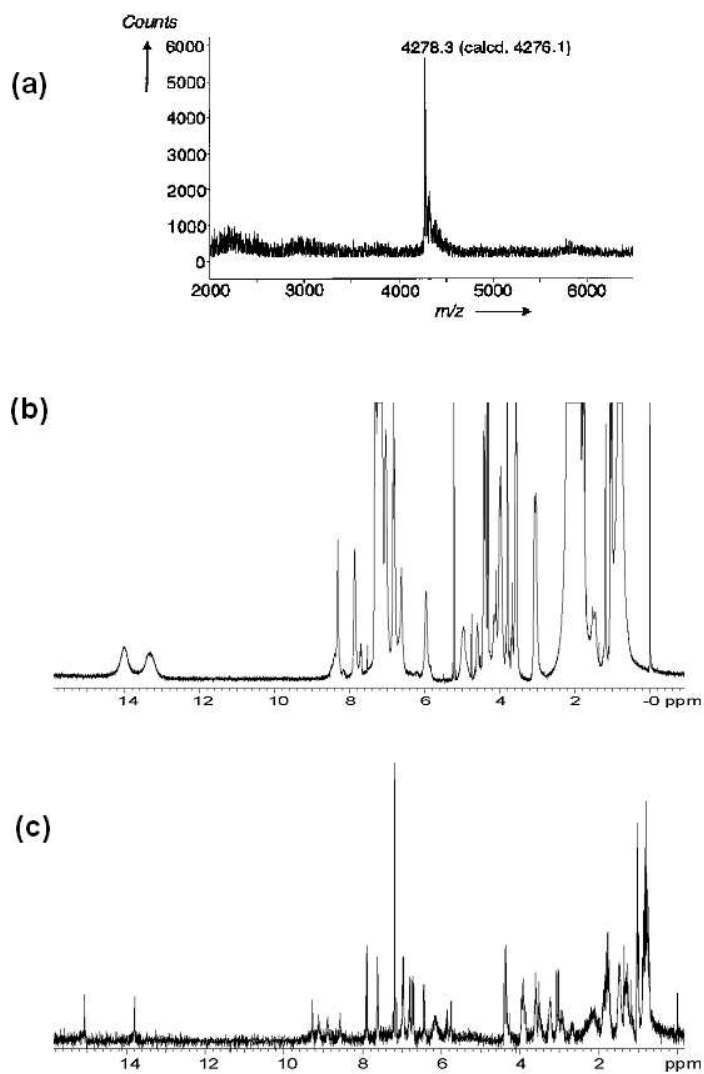


figure 2  
190x254mm (96 x 96 DPI)

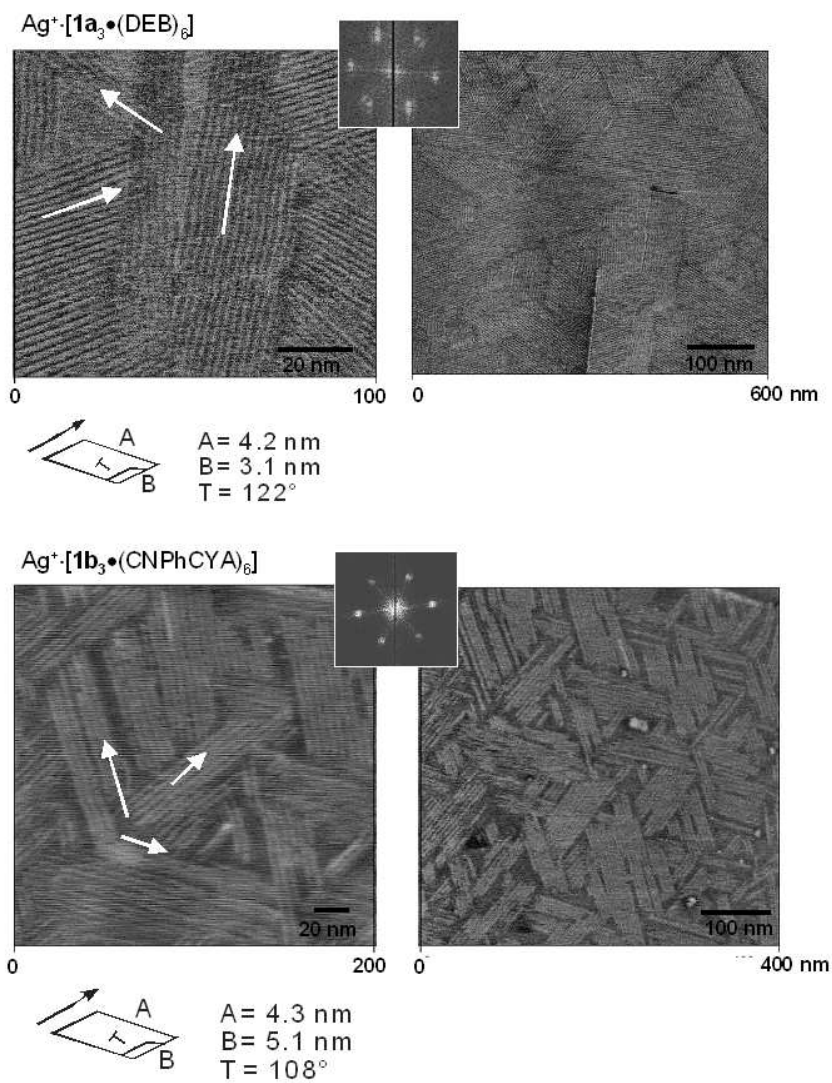


figure 3  
190x254mm (96 x 96 DPI)

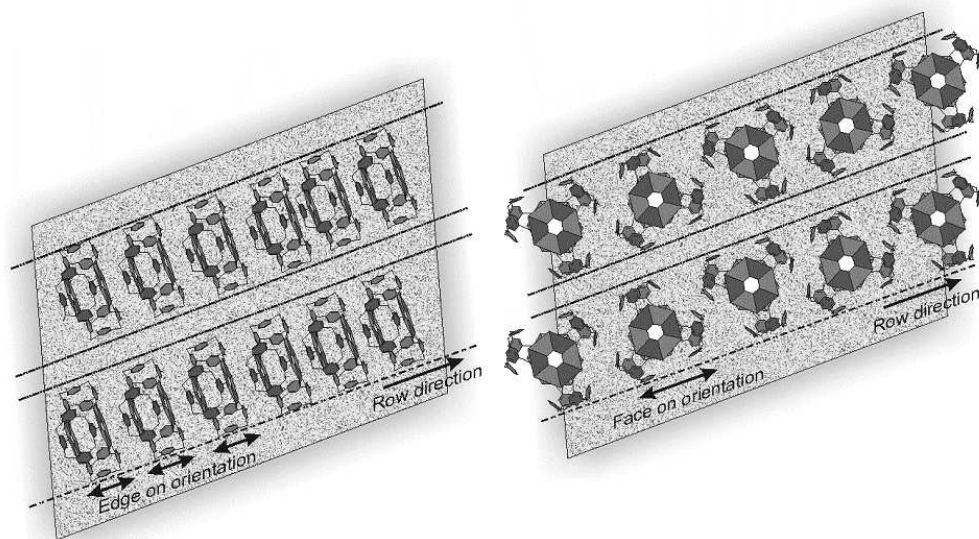


figure 4  
254x190mm (96 x 96 DPI)

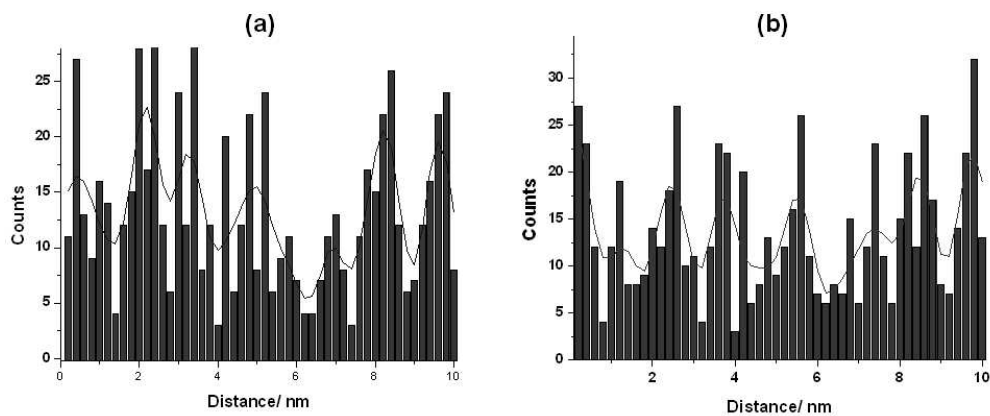


figure 5  
254x190mm (96 x 96 DPI)

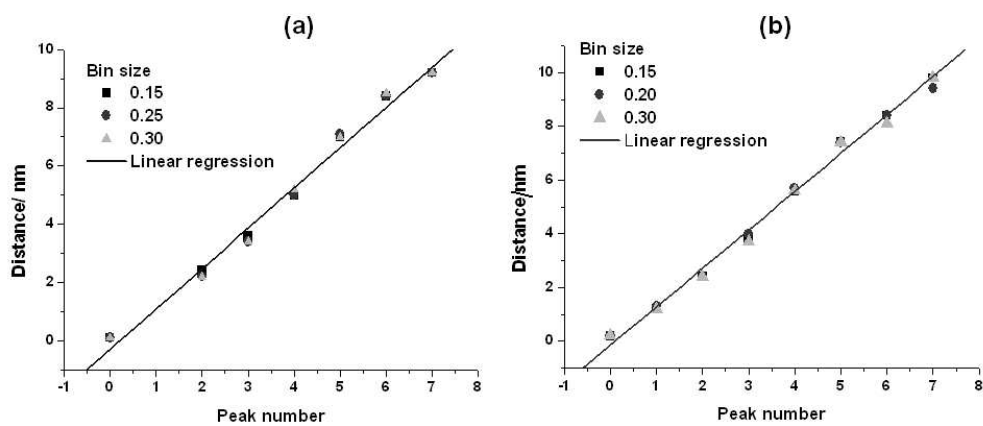


figure 6  
254x190mm (96 x 96 DPI)